The Journal of Physiology

# Low-voltage activated Kv1.1 subunits are crucial for the processing of sound source location in the lateral superior olive in mice

Anita Karcz[1], Matthias H. Hennig[2,3], Carol A. Robbins[4], Bruce L. Tempel[4], Rudolf Rübsamen[1] and Cornelia Kopp-Scheinpflug[1]

[1] *Institute of Biology, Faculty of Biosciences, Pharmacy and Psychology, University of Leipzig, Talstrasse 33, 04103 Leipzig, Germany*
[2] *Institute for Adaptive and Neural Computation, School of Informatics, University of Edinburgh, Edinburgh, UK*
[3] *Centre for Systems Biology at Edinburgh, C. H. Waddington Building, The Kings Buildings Campus, Edinburgh, UK*
[4] *VM Bloedel Hearing Research Center and Department of Otolaryngology, University of Washington, Seattle, WA, USA*

**Non-technical summary** Voltage-gated potassium channels control excitability throughout the nervous system and their dysfunction (or mutation) is associated with epilepsy and movement disorders. Loss of the insulating myelin sheath around nerve fibres (axons) in multiple sclerosis causes transmission failure by exposing too many potassium channels. We show that too few potassium channels also causes errors in information transmission as measured by the ability to localize the source of a sound, and suggests a general role for potassium channels along myelinated nerve fibres. These results give insights into normal neuronal function and into neurodegenerative disease mechanisms for patients with ataxia and multiple sclerosis.

**Abstract** Voltage-gated potassium (Kv) channels containing Kv1.1 subunits are strongly expressed in neurons that fire temporally precise action potentials (APs). In the auditory system, AP timing is used to localize sound sources by integrating interaural differences in time (ITD) and intensity (IID) using sound arriving at both cochleae. In mammals, the first nucleus to encode IIDs is the lateral superior olive (LSO), which integrates excitation from the ipsilateral ventral cochlear nucleus and contralateral inhibition mediated via the medial nucleus of the trapezoid body. Previously we reported that neurons in this pathway show reduced firing rates, longer latencies and increased jitter in Kv1.1 knockout (*Kcna1*$^{-/-}$) mice. Here, we investigate whether these differences have direct impact on IID processing by LSO neurons. Single-unit recordings were made from LSO neurons of wild-type (*Kcna1*$^{+/+}$) and from *Kcna1*$^{-/-}$ mice. IID functions were measured to evaluate genotype-specific changes in integrating excitatory and inhibitory inputs. In *Kcna1*$^{+/+}$ mice, IID sensitivity ranged from +27 dB (excitatory ear more intense) to −20 dB (inhibitory ear more intense), thus covering the physiologically relevant range of IIDs. However, the distribution of IID functions in *Kcna1*$^{-/-}$ mice was skewed towards positive IIDs, favouring ipsilateral sound positions. Our computational model revealed that the reduced performance of IID encoding in the LSO of *Kcna1*$^{-/-}$ mice is mainly caused by a decrease in temporal fidelity along the inhibitory pathway. These results imply a fundamental role for Kv1.1 in temporal integration of excitation and inhibition during sound source localization.

(Resubmitted 30 November 2010; accepted after revision 5 January 2011; first published online 10 January 2011)
**Corresponding author** C. Kopp-Scheinpflug: MRC Toxicology Unit, University of Leicester, Leicester LE1 9HN, UK. Email: cks7@le.ac.uk

**Abbreviations** AP, action potential; CF, characteristic frequency; FG, hydroxystilbamidine; IC, inferior colliculus; ICC, immunocytochemical; IID, interaural intensity difference; ITD, interaural time difference; LSO, lateral superior olive; MNTB, medial nucleus of the trapezoid body; VCN, ventral cochlear nucleus.


DOI: 10.1113/jphysiol.2010.203331

## Introduction

Throughout the brain, voltage-gated potassium (Kv) currents contribute to action potential (AP) waveform, temporal precision of AP generation and neuron-specific AP firing patterns. The influence of Kv channels on integration of excitation and inhibition is explored in the auditory brainstem, where temporal precision is required for accurate spatial representation of the acoustic environment. To achieve this precision for stimuli with specific interaural time differences (ITDs) and interaural intensity differences (IIDs), low-voltage activated $K^+$ channels are highly expressed throughout the sound localization pathway (Wang *et al.* 1994; Grigg *et al.* 2000; Barnes-Davies *et al.* 2004). Kv channels containing the Kv1.1 subunit reduce AP jitter (Gittelman & Tempel, 2006) and determine AP threshold (Manis & Marx, 1991; Brew & Forsythe, 1995; Brew *et al.* 2003; Klug & Trussell, 2006; Cao *et al.* 2007; Oertel *et al.* 2008), which are key features of the ITD–IID-based encoding of sound source location. Mice have little hearing sensitivity below 3 kHz, and their small head size means that naturally occurring ITDs are too small to be encoded unambiguously. Hence, the low frequency ITD-based localization pathway involving the medial superior olive is likely to be less well developed (Ollo & Schwartz, 1979; Kuwabara & Zook, 1992). Instead, integration of IIDs (induced by the head shadow for high frequency sounds) provides crucial binaural information about the location of a sound source. Neurons in the lateral superior olive (LSO) are the first IID-sensitive cells in the mammalian ascending auditory pathway (Boudreau & Tsuchitani 1970; Irvine, 1992; Yin, 2002; Tollin, 2003; Kandler *et al.* 2009). They receive excitatory glutamatergic input from the ipsilateral ventral cochlear nucleus (VCN) and inhibitory glycinergic input from the medial nucleus of the trapezoid body (MNTB), which itself is driven by the contralateral VCN (Osen, 1969; Glendenning *et al.* 1985; Spangler *et al.* 1985; Finlayson & Caspary, 1991; Smith *et al.* 1991, 1998). IID processing is achieved by integrating ipsilateral excitatory and contralateral inhibitory inputs which must converge with submillisecond precision (Joris & Yin, 1995). We have previously shown that in mice lacking the *Kcna1* gene (encoding the Kv1.1 subunit) AP counts were reduced, while latency and jitter were increased in MNTB neurons (Kopp-Scheinpflug *et al.* 2003). Based on these findings we postulate an altered IID processing in the LSO of *Kcna1*$^{-/-}$ mice due to a weakened, delayed and temporally less precise inhibitory input from the longer conducting pathway originating in the contralateral ear.

We tested the significance of Kv1.1-containing channels in binaural processing of IIDs under physiological conditions by performing extracellular single-unit recordings from the LSO of *Kcna1*$^{-/-}$ mice and littermate controls *in vivo*. Computational modelling of the relative timing and strength of the inputs suggests increased AP-jitter of the inhibitory input as the main reason for the impaired encoding of sound location in Kv1.1 knockout mice.

## Methods

### Mouse strains and genotyping

The experiments were performed at the Neurobiology Laboratories of the Faculty of Bioscience, Pharmacy and Psychology of the University of Leipzig (Germany). All experimental procedures were approved by the Saxonian District Government, Leipzig, and were conducted according to European Communities Council Directive of 24 November 1986 (86/609/EEC). The *Kcna1*$^{tm1Tem}$ strain was generated as described in Smart *et al.* (1998). Chimerical founders were crossed and maintained in serial backcrosses to C3HeB/FeJ females, purchased from The Jackson Laboratory (Bar Harbor, ME, USA). Mice used in this study were generated by intercrossing heterozygotes from the C3HeB/FeJ-*Kcna1*$^{tm1Tem}$ line maintained at the University of Leipzig. Mice were kept on a 12 h light–dark cycle with food and water freely available. Male and female mice used for these experiments were on average 28 days old.

Genotyping was carried out on DNA isolated from tail clips of each mouse in a litter aged 7–10 days as described by Brew *et al.* (2003). Detailed protocols are available online (http://depts.washington.edu/tempelab/Protocols/KCNA1.html).

### Immunocytochemistry

*Kcna1*$^{+/+}$ and *Kcna1*$^{-/-}$ mice were obtained from a colony maintained at the University of Washington. All animal procedures were listed in an approved protocol by the Institutional Animal Care and Use Committee at the University of Washington and were conducted in compliance with the NIH *Guide for the Care and Use of Animals*. The mice were deeply anaesthetized with Nembutal (100 mg kg$^{-1}$) prior to transcardial perfusion on postnatal day 35. They were perfused with 0.9% saline with heparin (1000 units ml$^{-1}$ saline), for 1 min, followed by 15 min of cold 4% paraformaldehyde fixative solution in 0.1 M phosphate buffered saline (PBS; pH 7.4). The brains were removed and washed in 0.1 M PBS overnight, cryoprotected in 10% sucrose in 0.1 M PBS for 1 h, and 30% sucrose in 0.1 M PBS for 24 h at 4°C, followed by Optimal Cutting Temperature compound (Tissue-Tek; Sakura Finetek, Torrance, CA, USA). The brain tissue was then frozen on dry ice, cryostat sectioned coronally at 20 $\mu$m, mounted on microscope slides and stored at 4°C.

Immunocytochemical (ICC) labelling methods were used on auditory brainstem tissue from *Kcna1*$^{+/+}$ and *Kcna1*$^{-/-}$ mice to localize channels containing Kv1.1 and Kv1.2 subunits in the LSO. Tissue sections were washed in PBS, and treated with pepsin (Lorincz & Nusser, 2008) at a concentration of 0.2 mg ml$^{-1}$ pepsin (Dako, Houston, TX, USA) in 0.2 M HCl at 37°C for 12–15 min. After rinsing, the tissue was immersed in a blocking solution of 0.3% sodium borohydride in PBS for 15 min. Following three 10 min washes in PBS, the tissue was pre-incubated in PBS with 0.1% Tween and 0.03% saponin for 10 min, and then incubated for 1 h in MOM blocking agent (Mouse on Mouse Immunodetection Kit; Vector Laboratories, Inc., Burlingame, CA, USA). Sections were then incubated in primary antibodies from NeuroMab (UC Davis/NIH NeuroMab facility): mouse monoclonal anti-Kv1.1 (K36/15) and anti-Kv1.2 (K14/16), both $IgG_{2b}$ isotype specific. The antibodies were diluted in PBS with MOM Protein (MOM Kit; Vector Laboratories) along with 0.1% Triton X-100 and 0.03% saponin. The Kv1.1 (1:2000) antibody was incubated for 15–20 h, and Kv1.2 (1:3800) was incubated for 30–36 h at 4°C. Following several rinses with PBS, Alexa Fluor488 goat anti-mouse ($IgG_{2b}$ isotype specific), was used as the secondary antibody to visualize the immunoreactions (1:500, Invitrogen, Carlsbad, CA, USA). The antibody was diluted in a blocking solution with 5% NGS (Vector Laboratories, S-1000), and tissue was incubated for 3–5 h at room temperature, and washed in PBS at least three times 10 min prior to coverslipping the slides with Vectashield mounting medium for fluorescence with DAPI (Vector Laboratories, H-1200).

Additional sections were double-labelled with $Na_V1.6$ rabbit polyclonal primary antibody (1:100, Alomone Labs Ltd, Jerusalem, Israel, ASC-009) together with the Kv1.1 mouse monoclonal antibody (NeuroMab) as above. After several rinses, sections were incubated with biotinylated goat anti-rabbit (1:300, Vector Laboratories) and Alexa Fluor488 $IgG_{2b}$ (1:500, Invitrogen) goat anti-mouse secondary antibodies for 2 h. Following several rinses, sections were incubated in Streptavidin 633 (1:500, Invitrogen) and Alexa Fluor488 $IgG_{2b}$ (1:500, Invitrogen) goat anti-mouse secondary antibodies for an additional 1.5 h followed by rinsing prior to coverslipping.

A confocal laser scanning microscope (FV 1000, Olympus) was used for collection of images using a 20× (NA/0.75) dry objective lens, or a 100× (NA/1.40) oil immersion objective lens. ImageJ (v. 1.42, National Institutes of Health, Bethesda, MD, USA) and Adobe Photoshop were used to create maximum intensity projections and figures. No labelling was seen in control experiments, where primary antibodies were excluded from ICC solutions. Kv1.1 antibody expression was not observed in auditory brainstem tissue from *Kcna1*$^{-/-}$ mice; however, Kv1.2 labelling was observed in tissue from these mice (Fig. 2*A*–*H*).

## *In vivo* electrophysiology

**Surgical preparation.** During the experiments and surgical preparation, the animals were anaesthetized with a combined initial dose of 0.01 ml (g body weight)$^{-1}$ of ketamine hydrochloride (100 mg (kg body weight)$^{-1}$; Parke-Davis, Berlin, Germany) and xylazine hydrochloride (5 mg (kg body weight)$^{-1}$; Bayer, Leverkusen, Germany). Anaesthesia was maintained throughout the recording experiments by hourly injections of one-third of the above dose. The skull of an experimental animal was exposed along the dorsal midsagittal line, and a small metal bolt for supporting the animal in the stereotaxic recording device was glued to the bone overlaying the forebrain. Two holes were drilled in the skull 2000–2300 $\mu$m caudal to the lambda suture, which correspond to positions above the rostral third of the cerebellum. The first drill hole, located 1500 $\mu$m lateral to the midline, was used to position the reference electrode in the superficial cerebellum. For the insertion of recording electrodes, the second drill hole (500 $\mu$m diameter) was located over the midline, and the electrodes were angled at 10–15 deg to the midsagittal plane.

**Acoustic stimulation.** Auditory stimuli were generated at a sampling rate of 97.7 kHz using custom written software (Rec_thor; Dr M. Weick, University of Leipzig) on a standard PC. Stimuli were then transferred to a real-time processor (RP2.1, Tucker Davis Technology (TDT), Alachua, FL, USA), D/A converted and further sent to ED1 driven electrostatic speakers (EC1, TDT). In these, sound is emitted through small pipes onto which acoustic tubing was attached to deliver stimuli to the outer ear approximately 5 mm from the animal's eardrum. The frequency characteristic of the transducer was measured with a quarter inch condenser microphone (Bruel & Kjaer, Type 2619, Naerum, Denmark) coupled to a short plastic tube with an approximate volume of 0.1 ml mimicking the conditions of the outer ear. A computer controlled procedure determined the sound pressure levels at a defined input voltage for 50 frequencies per decade. The data were stored in a computer file that was used during experiments for online correction of stimulus intensities. The maximum output of the speakers was clipped to 90 dB SPL. No phase differences were present between stimuli of the two speakers.

## Data collection and analysis

All recording experiments were performed in a sound-attenuated chamber (Industrial Acoustics, type 400, Winchester, UK). During the experiments the body temperature was kept between 36°C and 37.5°C by positioning the animal on a temperature-controlled heating pad (Harvard Apparatus, Holliston, MA, USA)

and maintaining the temperature of the sound-attenuated chamber at 25 to 30°C.

**Multiunit mapping.** At the beginning of the recording session, stereotaxic coordinates of the LSO were determined by online analysis of acoustically evoked multiunit activity. As a point of reference, we first identified MNTB activity and oriented laterally from the caudal third of the MNTB until binaural acoustic stimulation evoked excitatory–inhibitory (E-I) response characteristics, typical for LSO (Fig. 1). Glass micropipettes (Clark Electromedical Instruments, Reading, UK) filled with 3 M KCl and having impedances of 1–5 MΩ were used. Employing monaural ipsilateral tone-burst stimulation, the characteristic frequencies (CFs) of multiunits were measured by a computer-automated procedure every 100 $\mu$m in several penetrations to delimit the physiological boarders of the LSO (test range 1–50 kHz and 0–90 dB SPL).

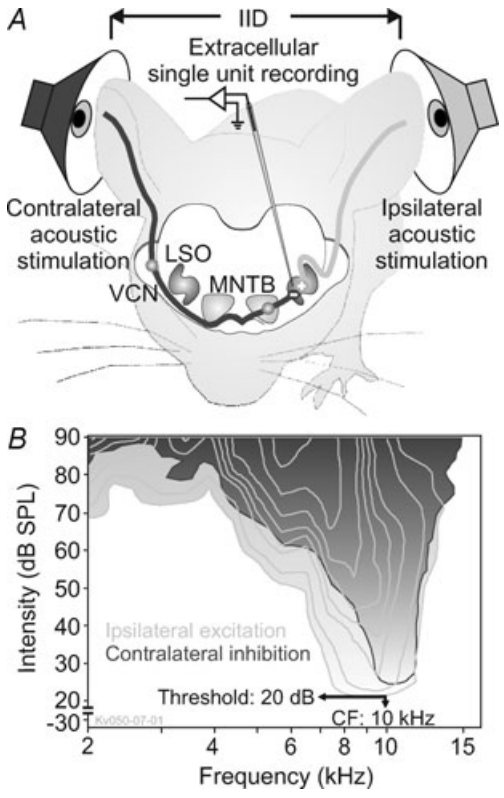


**Figure 1. IID pathway of the mouse brainstem**
*A*, sketch of the mouse brainstem IID pathway, binaural acoustic stimulation, and extracellular recordings from units in the LSO. *B*, response maps of one representative wild-type LSO unit in response to ipsilateral (light grey) or contralateral (dark grey) acoustic stimulation. The respective outermost lines show the frequency/intensity ranges that correspond to significant increase (excitation, light grey) or decrease (inhibition, dark grey) in firing rates relative to the units' spontaneous rates. Additional contour lines show significant further increase or decrease of firing rates. The unit's CF and threshold were obtained from this analysis. This *Kcna1*$^{+/+}$ unit shows a strong overlap of excitatory and inhibitory response areas with largely identical CFs and thresholds. In some units, the inhibitory response area was much broader tuned than the excitatory one (not shown).

**Single-unit recordings.** Following multiunit mapping, recordings from single units were made through high impedance glass micropipettes (10–30 MΩ). The activity of isolated single units was bandpass filtered (0.45–7 kHz) and amplified (NeuroData IR-183, Cygnus Technologies Inc., Delaware Water Gap, PA, USA; PC1, TDT) to the voltage range of the spike discriminator (SD1, TDT) and the A/D converter (RP2.1, TDT). Single units were identified by their relatively constant spike height and waveform and a large signal-to-noise ratio. The discriminated spike times were acquired with a sampling rate of 10 $\mu$s using custom-written software (Rec˙thor; Dr M. Weick, University of Leipzig).

**Analysis of spike recordings.** The excitatory response map for each unit was measured by random presentation of pure-tone pulses (100 ms duration, 5 ms rise-fall time, 100 ms interstimulus interval) within a given matrix of $16 \times 15$ frequency/intensity pairs (240 combinations). The frequency range of this matrix typically included five octaves (4 tones/octave) with about three octaves below the estimated CF and two octaves above. The intensity varied in 5 dB-steps between 90 and 20 dB SPL. Each frequency/intensity combination was presented five times in a predefined frequency/intensity array (1200 tone bursts). The timing and number of spikes were measured during the 100 ms period of stimulus presentation. Spontaneous activity was defined by the firing rate during eighty 100 ms periods (8 s) with maximal attenuation (120 dB) of the stimulus randomly inserted in the stimulus protocol. Typical response areas of an LSO neuron are shown in Fig. 1*B*. An excitatory response area (marked in light grey in Fig. 1*B*) was defined by the range of frequency/intensity combinations that evoked firing rates at or above the 10% significance level above spontaneous activity (Dorrscheidt, 1981). The outline of the response area defined the unit's frequency-threshold curve, from which the CF and the threshold at CF were determined. Vice versa, inhibitory response areas were defined by a respective reduction of firing rates below the level of spontaneous rate (marked in dark grey in Fig. 1*B*). Each successive contour line represents an additional significant increase or decrease in firing. The sharpness of frequency tuning was determined at 10 dB above threshold by the $Q_{10}$ value (CF/bandwidth). Rate-level functions were calculated at CF by averaging the spike rates at each stimulus intensity (5 repetitions/stimulus). Median latency and jitter defined as the 25–75% quartile range were computed for the first spikes after the onset of the

acoustic stimulus averaged over 250 repetitions. Temporal response patterns of the neurons were quantified by the median interspike interval (ISI) for the onset component (20 ms).

Sensitivity to IIDs was tested by presenting a constant tone (40 ms) at CF, 20 dB (±15 dB) above threshold to the ipsilateral ear (using these parameters, identical firing rates could be achieved in both genotypes) and simultaneously stimulating the contralateral ear at CF with stimulus intensities pseudo-randomly varying from 20 to 90 dB SPL in 5 dB-steps. The acquired averaged IID functions (25 repetitions) were normalized, with AP firing rates during monaural ipsilateral stimulation corresponding to 100%. For further quantification, IID functions were fit with four-parametric sigmoid functions from which half maximal IID values ($IID_{50}$) were determined.

Statistical analyses of the data were performed with SigmaStat or SigmaPlot (Systat Software Inc., San Jose, CA, USA). Unless indicated otherwise, results are expressed as means ± standard error of the mean (S.E.M.) or for non-normal distributions as median [25%; 75% quartiles]. For normally distributed data, statistical significance was assessed using the Student's *t* test or paired *t* test. For non-normal distributions, significance was assessed using the Wilcoxon's signed rank test or the Mann–Whitney rank sum test.

**Verification of recording sites.** In each animal, all recording sites were verified histologically by iontophoretic injections (2 $\mu$A for 5 min) of horseradish peroxidase (HRP) or hydroxystilbamidine (FG; Biotium; equivalent to FluoroGold) at the end of the recording session. The mice were allowed to recover from anaesthesia and after 24 h (HRP) or 5 days (FG) the animals received a lethal anaesthetic injection and were then perfused via the left ventricle with 0.9% NaCl solution followed by fixative (2.5% paraformaldehyde in 0.1 M phosphate buffer, pH 7.4) for 20–25 min. The brain was sectioned on a vibrating blade microtome and the tissue sections (30 $\mu$m thick) were processed using the 3,3′-diaminobenzidine reaction to visualize the HRP mark (Adams, 1981). Following staining with cresyl violet, the tissue sections were examined under the light microscope, and the electrode tracks and recording sites were identified. FG tissue sections were examined with a fluorescence microscope (Zeiss, Axioskop, absorption/emission: 361/536 nm).

## Computational model

An LSO neuron was modelled as a single-compartment leaky integrate and fire unit with conductance-based synaptic inputs. The membrane potential $V$ is calculated by:

$$\tau_m \dot{V} = \sum_i g_i(t)(V - E_i) + \sum_c g_c(V - E_c) - (V - V_r),$$

with excitatory, ipsilateral and inhibitory, contralateral synaptic conductances $g_i(t)$ and $g_c(t)$. Note that in this equation conductances are expressed in units of the leak, and are therefore dimensionless. The membrane time constant was $\tau_m = 2$ ms (Wu & Kelly, 1991; Sanes & Takacs, 1993), the resting potential $V_r = -65$ mV, and the reversal potentials $E_i = 0$ mV for the ipsilateral and $E_c = -70$ mV for the contralateral inputs. The LSO neuron receives 10 excitatory and eight inhibitory inputs (Sanes, 1990). Each synaptic connection was modelled as:

$$\tau_{\{i,c\}\{i,c\}} = g^m_{\{i,c\}}\delta(t - t_s) - g_{\{i,c\}},$$

where $t_s$ are the spike times, and $\tau_i = 1.4$ ms and $\tau_c = 4$ ms are time constants (Sanes, 1990), and peak conductances $g_i^m = 2$ and $g_c^m = 6$ for the ipsi- and contralateral inputs, respectively. The peak conductances were chosen such that a volley of spikes on the ipsilateral input could evoke a single postsynaptic AP in the absence of inhibition, and that complete inhibition could be achieved by approximately doubling the contralateral spike rate with respect to the ipsilateral input. A postsynaptic spike is generated, when the membrane potential exceeds the threshold $\Theta = -45$ mV, after which the membrane potential is reset to $-75$ mV.

Synthetic input spike trains were generated to reproduce the central properties of sound-evoked responses in VCN and MNTB neurons of wild-type and *Kcna1*$^{-/-}$ mice (Kopp-Scheinpflug *et al.* 2003). To simulate IID functions, all excitatory inputs were held at a constant spike rate $R_i$, while the rate of the inhibitory inputs were systematically varied from $R_c = 0$ Hz (pure ipsilateral stimulation) to $R_c = 2R_i$. Excitatory ipsilateral spikes were first generated as a regular sequence of spikes at a fixed rate and fixed first spike latency. Inhibitory spikes were generated by randomly removing spikes from regular spike trains at a rate $R_i$ if $R_c < R_i$, or at a rate of $2R_i$ if $R_c > R_i$. Then, spike jitter was introduced by in turn shifting each spike, and all successive spikes, by a random amount. Each random shift was drawn from an exponential distribution with a constant mean and standard deviation $\sigma_{\{i,c\}}$. If this resulted in an inter-spike interval shorter than an absolute refractory period ($t_r = 1$ ms), the second spike was removed. In all cases, the mean first spike latency was corrected by subtracting the corresponding mean from its pre-specified value. As a result, in each spike train the average first spike latency was always constant and the timing of successive spikes reflect the cumulative jitter of all previous spikes. To include level-dependent latency differences in MNTB neurons (FitzGerald *et al.* 2001; Kopp-Scheinpflug *et al.* 2003), the

relative inhibitory latency $\Delta t$ was further adjusted by a delay of $\delta_t = -(R_c/R_i - 1) \times 1.25$ ms.

IID functions were obtained by measuring the average firing rate of the simulated LSO neuron in 15 repetitions of a 40 ms stimulus at different ratios of ipsilateral and contralateral inputs. All differential equations were integrated with the forward Euler method with a time step of 10 $\mu$s, using Matlab (v. 7.5; The Mathworks, Natick, MA, USA).

## Results

Recordings were obtained from 59 (28 *Kcna1*$^{+/+}$, 31 *Kcna1*$^{-/-}$) IID-sensitive LSO neurons from 10 *Kcna1*$^{-/-}$ mice and seven littermate controls. Immunocytochemical staining confirmed that Kv1.1-containing channels are well expressed throughout the *Kcna1*$^{+/+}$ LSO (Fig. 2*A*), although a tonotopic gradient, as described for the rat LSO (Barnes-Davies *et al.* 2004), could not be confirmed in mice. Juxtaparanodal Kv1.1 staining in the fibres surrounding the LSO neurons suggests their importance for maintaining axonal conduction (Fig. 2*B*). *Kcna1*$^{-/-}$ mice showed Kv1.1 staining neither in the LSO nor along their afferent input pathways verifying the complete knockout of Kv1.1 (Fig. 2*C* and *D*). Immunostaining for the Kv1.2 subunit, which heteromultimerizes with Kv1.1 showed that the LSO and the processes in both genotypes had apparently normal morphology and Kv1.2 expression (Fig. 2*E*–*H*). The juxtaparanodal localization of Kv1.1 channels in *Kcna1*$^{+/+}$ mice is confirmed by subcellular expression of voltage-gated sodium channels ($Na_V1.6$) in mature nodes of Ranvier, providing a typical triplet staining (Fig. 2*I* and *J*). $Na_V1.6$ channels are also present in *Kcna1*$^{-/-}$ mice (Fig. 2*K* and *L*).

### *Kcna1*$^{-/-}$ mice lack IID sensitivity corresponding to contralateral sound positions

Previous studies of *Kcna1*$^{-/-}$ mice with an intact auditory system reported proportional impairment in timing and firing rate, with a minor effect in the excitatory pathway (into the LSO via the VCN) and a larger effect in the

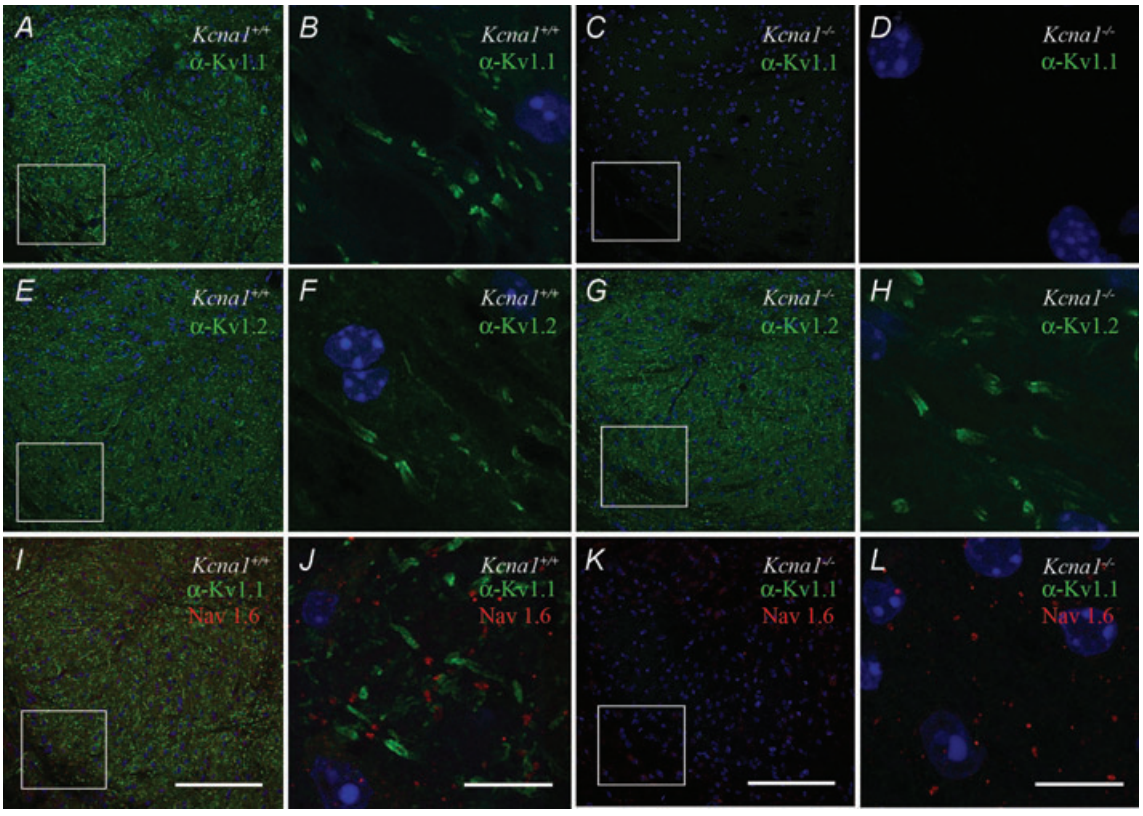


**Figure 2. Kv1 expression in the mouse LSO**
*A* and *B*, immunolabelling revealed both cellular and axonal Kv1.1 labelling in *Kcna1*$^{+/+}$ tissue (*A* and *B*), while no Kv1.1 expression was found in *Kcna1*$^{-/-}$ tissue (*C* and *D*); nuclei were visualized with DAPI. There was intense staining of Kv1.2 in both *Kcna1*$^{+/+}$ (*E* and *F*) and *Kcna1*$^{-/-}$ tissue (*G* and *H*). Co-labelling of juxtaparanodal Kv1 with nodal $Na_V1.6$ showed the typical triplet staining of the nodes of Ranvier in wild-type tissue (*I* and *J*) but not in *Kcna1*$^{-/-}$ tissue (*K* and *L*). In the latter, only $Na_V1.6$ staining is present besides the DAPI. Low magnification images (20×) are shown in *A*, *C*, *E*, *G*, *I* and *K*; squares indicate areas magnified in *B*, *D*, *F*, *H*, *J* and *L*, respectively. Scale bars: low magnification: 100 $\mu$m, high magnification: 10 $\mu$m.

inhibitory pathway via the MNTB (Kopp-Scheinpflug *et al.* 2003). To investigate the consequences of the differential changes along these two input pathways for the integration in LSO neurons, we analysed IID sensitivity in *Kcna1*$^{-/-}$ and wild-type mice.

All LSO units in both genotypes responded with highest firing rates to sound stimulation favouring the ipsilateral ear (positive IIDs; Fig. 3*A* and *B*). Increasing the sound intensity at the contralateral ear (towards negative IIDs) progressively reduced the number of ipsilaterally evoked APs (Fig. 3*B*). We compared normalized IID functions of 28 *Kcna1*$^{+/+}$ (Fig. 3*C*) and 31 *Kcna1*$^{-/-}$ neurons (Fig. 3*D*) and found the IID functions of *Kcna1*$^{+/+}$ neurons to cover the range of IIDs which a small headed species such as the

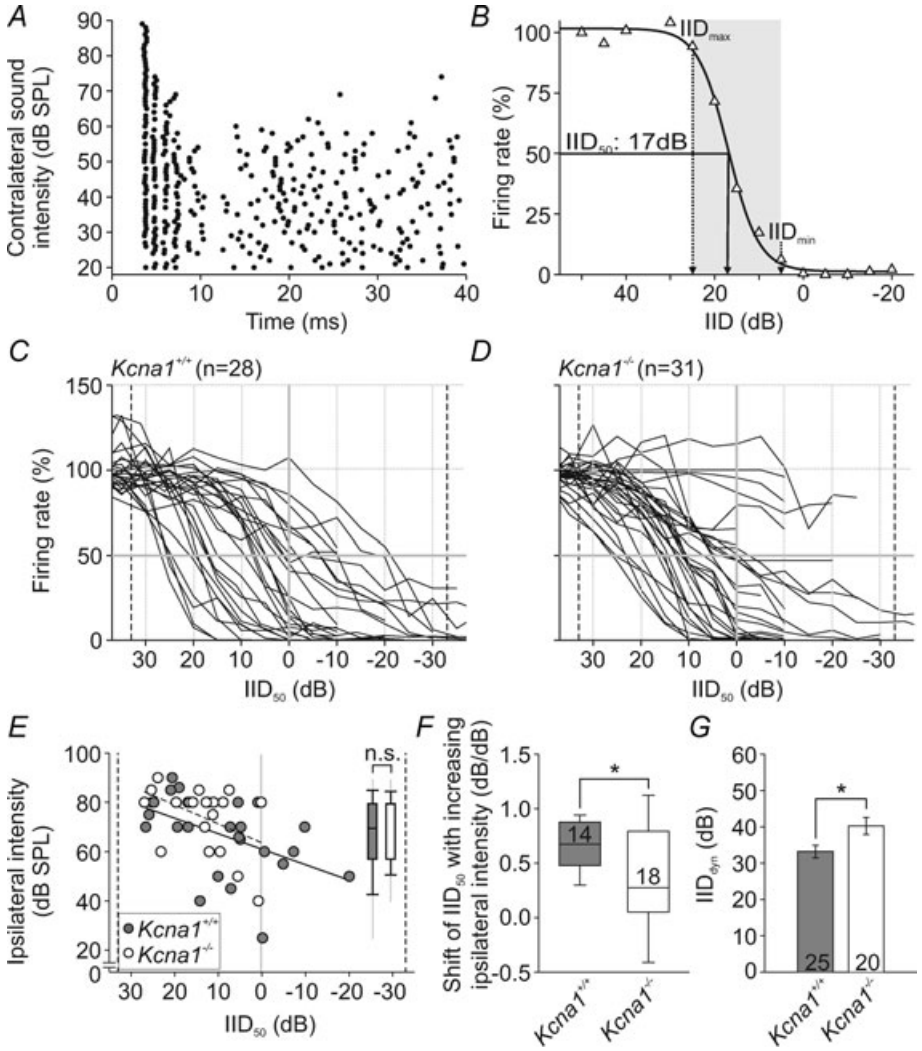


**Figure 3. IID encoding in *Kcna1*$^{+/+}$ and *Kcna1*$^{-/-}$ mice**
*A*, dot raster display of the response of a representative unit to binaural stimulation (40 ms; CF at the respective ear); ipsilateral: 20 dB above threshold; contralateral: levels between 0 and 90 dB SPL in steps of 5 dB (presented in pseudorandom order; ordinate). Note that the firing rate decreased with increasing contralateral stimulus intensities. *B*, normalized firing rate (same unit as in *A*) plotted for different IIDs, i.e. ipsilateral minus contralateral intensity: positive IIDs representing higher ipsilateral and negative IIDs higher contralateral stimulus levels. Firing rate at ipsilateral stimulation exclusively was set to 100%. Data points were fitted by a 4-parametric sigmoid function (continuous line). From such fits, IID values corresponding to a 50% rate reduction ($IID_{50}$) and the dynamic range of the IID functions (grey shaded area) were determined for further analyses. *C* and *D*, IID functions obtained from the LSO of *Kcna1*$^{+/+}$ (*C*) and *Kcna1*$^{-/-}$ mice (*D*). While in the *Kcna1*$^{+/+}$ LSO, IID functions are equally distributed between negative and positive IIDs, in *Kcna1*$^{-/-}$ mice, IID functions do not seem to achieve 50% rate reduction for negative IIDs. This is also shown by the uneven distribution of $IID_{50}$ values between both genotypes (*E*). The inset in *E* features the range of absolute ipsilateral intensities used for the recording of IID functions in wild-type (grey) and knockout (white) LSO. *F*, within recordings from individual neurons, $IID_{50}$ values shifted towards more positive IIDs with increasing ipsilateral intensity. This increase was significantly larger in wild-types (grey). *G*, the *Kcna1*$^{-/-}$ IID dynamic ranges (white) were larger and accompanied by shallower slopes.

**Table 1. Response features of IID sensitive LSO units**

| | *Kcna1*$^{+/+}$ | | | | | *Kcna1*$^{-/-}$ | | | | | | |
|---|---|---|---|---|---|---|---|---|---|---|---|---|
| Parameter | Mean ± S.E.M. | Median | 25% | 75% | *n* | Mean ± S.E.M. | Median | 25% | 75% | *n* | Test | Significance |
| $IID_{50}$ (dB) | 9.7 ± 2.4 | 7.3 | 3.9 | 19.7 | 25 | 13.6 ± 1.7 | 12.6 | 9.3 | 18.1 | 20 | MWRS-test | $P = 0.278$ |
| $IID_{dyn}$ (dB) | 33 ± 2 | 35 | 29 | 40 | 25 | 40 ± 2 | 40 | 35 | 50 | 20 | *t* test | $P = 0.017$ |
| $CF_{exc}$ (kHz) | 19.4 ± 2.3 | 13.4 | 10.5 | 27.0 | 28 | 15.2 ± 1.4 | 12.6 | 9.1 | 23.0 | 31 | MWRS-test | $P = 0.233$ |
| $CF_{inh}$ (kHz) | 18.8 ± 2.4 | 16.2 | 10.5 | 23.2 | 18 | 19.6 ± 2.5 | 19.1 | 9.0 | 27.0 | 22 | MWRS-test | $P = 0.989$ |
| $Q_{10}$ | 1.89 ± 0.22 | 1.54 | 1.08 | 2.61 | 28 | 1.49 ± 0.22 | 1.33 | 0.74 | 1.77 | 31 | MWRS-test | $P = 0.103$ |
| Spont. rate (spikes $s^{-1}$) | 2.5 ± 1.1 | 0.4 | 0.0 | 1.8 | 28 | 3.6 ± 1.9 | 0.1 | 0.0 | 0.9 | 31 | MWRS-test | $P = 0.344$ |
| Max. rate (spikes $s^{-1}$) | 168.1 ± 16.2 | 167.7 | 71.7 | 242.0 | 28 | 137.3 ± 18.5 | 128.0 | 46.3 | 212.5 | 31 | MWRS-test | $P = 0.116$ |
| $Threshold_{exc}$ (dB SPL) | 47 ± 3 | 50 | 34 | 59 | 28 | 56 ± 3 | 60.0 | 47 | 66 | 31 | MWRS-test | $P = 0.036$ |
| $Threshold_{inh}$ (dB SPL) | 43 ± 4 | 45 | 20 | 55 | 18 | 56 ± 3 | 58 | 45 | 70 | 22 | MWRS-test | $P = 0.028$ |
| Latency (ms) | 4.8 ± 0.5 | 4.0 | 3.7 | 4.6 | 25 | 5.2 ± 0.3 | 4.6 | 3.9 | 5.8 | 27 | MWRS-test | $P = 0.056$ |
| Jitter (ms) | 1.3 ± 0.7 | 0.3 | 0.1 | 0.6 | 25 | 1.1 ± 0.3 | 0.4 | 0.2 | 1.6 | 27 | MWRS-test | $P = 0.079$ |
| $ISI_{onset}$ (ms) | 3.55 ± 0.56 | 2.62 | 2.04 | 3.68 | 25 | 4.43 ± 0.59 | 3.18 | 1.81 | 6.71 | 27 | MWRS-test | $P = 0.297$ |

mouse could possibly encounter in a natural environment (Fig. 3*C*; Chen *et al.* 1995). In contrast, IID functions of *Kcna1*$^{-/-}$ neurons are limited to positive IIDs which would correspond to ipsilateral sound positions (Fig. 3*D*). To quantify the neurons' IID sensitivity, a four-parametric sigmoid function was fitted to the measured IID curves (Tollin *et al.* 2008). For further analysis data were only considered if the fit had a minimum of 95% correlation (online Supplemental Material) and no sign of crosstalk via bone conduction was observed. The latter would show up as a secondary increase in firing rate for very high contralateral intensities. The $IID_{50}$ value was defined as the IID resulting in a 50% reduction in maximum firing rate (Fig. 3*E*). Mean $IID_{50}$ values did not differ between genotypes ($P = 0.278$; Table 1) but their distribution was significantly restricted ($P \leq 0.05$) in *Kcna1*$^{-/-}$ mice.

Since the LSO rate-IID functions vary with changes in overall sound intensity, we plotted the ipsilateral intensity used for obtaining the IID curve (i.e. 20 dB above threshold) for each neuron of either genotype *versus* their respective $IID_{50}$ (Fig. 3*E*). We observed a dependency of $IID_{50}$ values on ipsilateral intensity that confirmed the relationship described in the literature (Tsai *et al.* 2010). Still, even though the absolute ipsilateral intensities in the *Kcna1*$^{-/-}$ mice cover a smaller range, they are not different from those used for the wild-type experiments (inset Fig. 3*E*; Table 1, Supplemental Material). Wild-type neurons clearly show a shift in $IID_{50}$ of 0.68 per dB increase in ipsilateral intensity (Fig. 3*F*). In the *Kcna1*$^{-/-}$ LSO units, however, we saw a significantly smaller shift of $IID_{50}$ with increasing ipsilateral sound levels (0.27 dB/dB; $P = 0.018$, Fig. 3*F*). So, despite this correlation between absolute intensity and $IID_{50,}$ the wide range of $IID_{50}$ (from −20 to +27) in wild-type mice contrasts with the restricted $IID_{50}$ range in *Kcna1*$^{-/-}$ mice (from +0 to +27).

In 76% of the wild-type neurons the contralateral inhibitory input was stronger than the excitatory input, resulting in positive $IID_{50}$ values, whereas in 24% of the neurons the excitation could only be inhibited by more intense inhibitory stimuli (negative $IID_{50}$). In contrast, only a few *Kcna1*$^{-/-}$ neurons showed $IID_{50}$ values close to 0 IID but not at negative IIDs (Fig. 3*E*). This restriction of IID sensitivity to positive IIDs might imply that inhibition in the knockout is more efficient, such that AP suppression is already present at low contralateral stimulus intensities. Or, alternatively, inhibition in the knockout may not be sufficient when driven at high rates (negative IIDs). This might explain why 23% of the *Kcna1*$^{-/-}$ neurons could not reach $IID_{50}$ (Fig. 3*C* and *D*). Neurons that are tuned to negative IIDs require a strong inhibitory input, a condition that might not be achieved in a large proportion of knockout neurons. One possibility to increase the strength of inhibition would be to increase intensity, but since the loudspeaker output was limited to 90 dB SPL, this could not be achieved in every case without introducing a ceiling effect.

Another option is to change the timing of the inhibitory input, by introducing a temporal lead for the contralateral sound in the knockout mice. Exploiting the phenomenon of time-intensity trading to increase inhibition efficiency, *Kcna1*$^{-/-}$ neurons indeed showed $IID_{50}$ where previously it had been absent (Supplemental Material). To evaluate the efficacy of inhibition we quantified the dynamic range of the IID functions ($IID_{dyn}$: range over which changes in IID induce significant changes in spike rates; shaded area in Fig. 3*B*). IID functions in *Kcna1*$^{+/+}$ neurons tended to have steeper slopes around $IID_{50}$, causing the average

$IID_{dyn}$ to be significantly smaller in the *Kcna1*$^{+/+}$ mice ($P = 0.017$; *Kcna1*$^{+/+}$: $33 \pm 2$ dB; *Kcna1*$^{-/-}$: $40 \pm 2$ dB; Fig. 3*G*). In *Kcna1*$^{-/-}$ cells IID functions were shallow, starting to decrease at significantly more positive IIDs (ipsilateral intensity > contralateral intensity; $IID_{max}$: *Kcna1*$^{+/+}$: 20 [16; 30] dB; *Kcna1*$^{-/-}$: 30 [25; 43] dB; $P = 0.011$; Fig. 3*B–D*). This suggests that the steeper the IID function (the smaller the $IID_{dyn}$), the more distinct the IID encoding by that neuron. Vice versa, in the *Kcna1*$^{-/-}$ mice, IID tuning is more shallow and therefore the encoding is less precise.

### Responses to ipsilateral excitatory inputs in *Kcna1*$^{-/-}$ mice are barely influenced by the lack of Kv1.1

Since in wild-type mice the Kv1.1 channel subunit is expressed along both the excitatory and the inhibitory pathway as well as in LSO neurons itself, the lack of sensitivity to negative IIDs for *Kcna1* knockouts could arise from each of the upstream processing levels. Differentiation of changes in the IID sensitivity arising in the LSO from inherited changes in the inputs was achieved by analysing the response characteristics to exclusively ipsilateral excitatory inputs.

Since the range of CFs was the same for both genotypes, we can assume that the sampled neuron population was similar (Table 1, Supplemental Material). The role of Kv1.1-containing channels in determining the excitability of LSO neurons was investigated by analysing sound driven and spontaneous firing rates. Spontaneous rates were generally low in LSO neurons of both genotypes with no significant difference between the two ($P = 0.344$; *Kcna1*$^{+/+}$: 0.4 [0.0; 1.8] spikes s$^{-1}$, $n = 28$; *Kcna1*$^{-/-}$: 0.1 [0; 0.9] spikes s$^{-1}$, $n = 31$; Table 1; Supplemental Material). LSO neurons must accurately differentiate evoked from spontaneous activity in order to act as interaural level detectors. This sound-evoked firing threshold was significantly elevated for the excitatory input of *Kcna1*$^{-/-}$ LSO ($threshold_{exc}$: $P = 0.036$; *Kcna1*$^{+/+}$: 50 [34; 59] dB SPL; *Kcna1*$^{-/-}$: 60 [47; 66] dB SPL; Table 1; Supplemental Material). Starting at the respective activation threshold, firing rates increased with ipsilateral stimulus intensity until reaching a plateau or decreasing again. Correct integration of excitation and inhibition requires an appropriate level of inhibition to balance the suprathreshold excitability. Therefore the absolute maximum firing rates were measured from the rate-level function at each neuron's CF; and these rates were found to be similar between *Kcna1*$^{-/-}$ and wild-type mice ($P = 0.116$; *Kcna1*$^{+/+}$: 168 [72; 242] spikes/s, $n = 28$; *Kcna1*$^{-/-}$: 128 [46; 213] spikes/s, $n = 31$; Table 1; Supplemental Material).

The rate-code of sound intensity is one aspect of IID processing by LSO neurons, but in addition accurate integration of excitation and inhibition requires temporal coincidence of inputs from both ears. Previous studies of auditory brainstem neurons have shown that Kv1.1-containing channels are essential for fast and precise onset firing to acoustic stimulation (Trussell, 1999; Bal & Oertel, 2001; Gittelman & Tempel, 2006). In the present study ipsilateral, excitatory stimuli evoked similar onset responses in the *Kcna1*$^{-/-}$ LSO neurons compared to the wild-type (latency: $P = 0.056$; *Kcna1*$^{+/+}$: 4.0 [3.7; 4.6] ms, $n = 25/28$; *Kcna1*$^{-/-}$: 4,6 [3.9; 5.8] ms, jitter: $P = 0.079$; *Kcna1*$^{+/+}$: 0.3 [0.1; 0.6] ms, $n = 25/28$; *Kcna1*$^{-/-}$: 0.4 [0.2; 1.6] ms $n = 27/31$; Table 1, Supplemental Material). In summary, the analysis of LSO responses to stimulation of the excitatory pathway revealed a 10 dB shift in threshold while all other parameters remained unchanged (Table 1). Hence, the change in the distribution of IID functions must originate in the inhibitory pathway.

### Contribution of the inhibitory input to IID encoding in *Kcna1*$^{-/-}$ mice evaluated by computational modelling

The inhibitory input to the LSO is not directly accessible by *in vivo* extracellular recording (because we cannot measure the IPSPs). An indirect measure of inhibition, however, is still possible by assessing the suppression of ipsilaterally evoked firing. Inhibitory response maps are acquired by presenting an excitatory stimulus 20 dB above threshold and simultaneously stimulating the inhibitory ear with various frequency/intensity combinations. This two-tone-tuning revealed similar inhibitory CFs for both genotypes ($CF_{inh}$: $P = 0.989$; *Kcna1*$^{+/+}$: 16.2 [10.5; 23.2] kHz; *Kcna1*$^{-/-}$: 19.1 [9.0; 27.0] kHz, Table 1; Supplemental Material). Inhibitory input thresholds were elevated to the same extent as those of the excitatory input; i.e. keeping threshold differences between both inputs stable in *Kcna1*$^{-/-}$ compared to *Kcna1*$^{+/+}$ mice ($threshold_{inhib}$: $P = 0.028$; *Kcna1*$^{+/+}$: 45 [20; 55] dB SPL; *Kcna1*$^{-/-}$: 58 [55; 70] dB SPL; Table 1; Supplemental Material).

Our previous electrophysiological results indicate that the temporal precision of inhibitory responses may play a role, but this cannot be assessed using extracelluar recording. Therefore we employed a computational model of an exemplary LSO neuron to address this issue. The model neuron was implemented as a leaky integrate-and-fire unit, using the neuronal properties of a wild-type LSO neuron (see Methods), which included the respective bilateral synaptic input. The properties of sound-evoked responses in VCN and MNTB neurons in *Kcna1*$^{+/+}$ and *Kcna1*$^{-/-}$ mice were simulated by creating synthetic input spike trains with the respective spike jitter and first-spike latencies that we observed in our preceding study (Kopp-Scheinpflug *et al.* 2003).

This model allowed us to separately study the effects of increased inhibitory jitter and latency and to identify the crucial temporal feature for precise and effective IID encoding. For evaluation of IID sensitivity, the spike rates of the simulated neuron were calculated for different combinations of fixed ipsilateral and variable contralateral input spike rates. An example of simulations with input spike train parameters typical for *Kcna1*$^{+/+}$ mice is shown in Fig. 4*A*–*C*. Here, the ratio of ipsilateral *vs.* contralateral spike rates was systematically increased, and the spike threshold of the LSO neuron was adjusted such that every volley of ipsilateral input spikes leads to a response, unless the inhibitory inputs are sufficiently strong to prevent a suprathreshold LSO response. When inhibition is weak (ratio contra/ipsi: 0–0.75), it arrives with a delay and does not coincide with excitatory synaptic input. Under these conditions the LSO neuron always follows the ipsilateral excitatory input. At the point where the contralateral firing rate matches that of the ipsilateral input, inhibition becomes more effective, and the response of the LSO gradually decreases (Fig. 4*B*, *C*). For a strong contralateral input, the inhibitory conductance is tonically active (Fig. 4*A*), and eventually this prevents all AP firing in the LSO neuron. No simple manipulation such as modifying the relative input strength or number of inputs will change this tuning (not illustrated). Therefore, as suggested previously (Reed & Blum, 1990; Park *et al.* 1996), tuning to different IIDs in LSO neurons is likely to be achieved by different combinations of ipsi- and contralateral thresholds, or rate-level relationships. For instance, an LSO neuron with negative IID should have an MNTB input with a less steep rate-level relation than the VCN input. The converse would be the case for positive IIDs.

High sound intensities usually evoke high firing rates but also induce a decrease in first spike latency (FitzGerald *et al.* 2001; Kopp-Scheinpflug *et al.* 2003). Such a latency decrease for a strong contralateral input must also be considered to achieve a full inhibition of AP firing in the

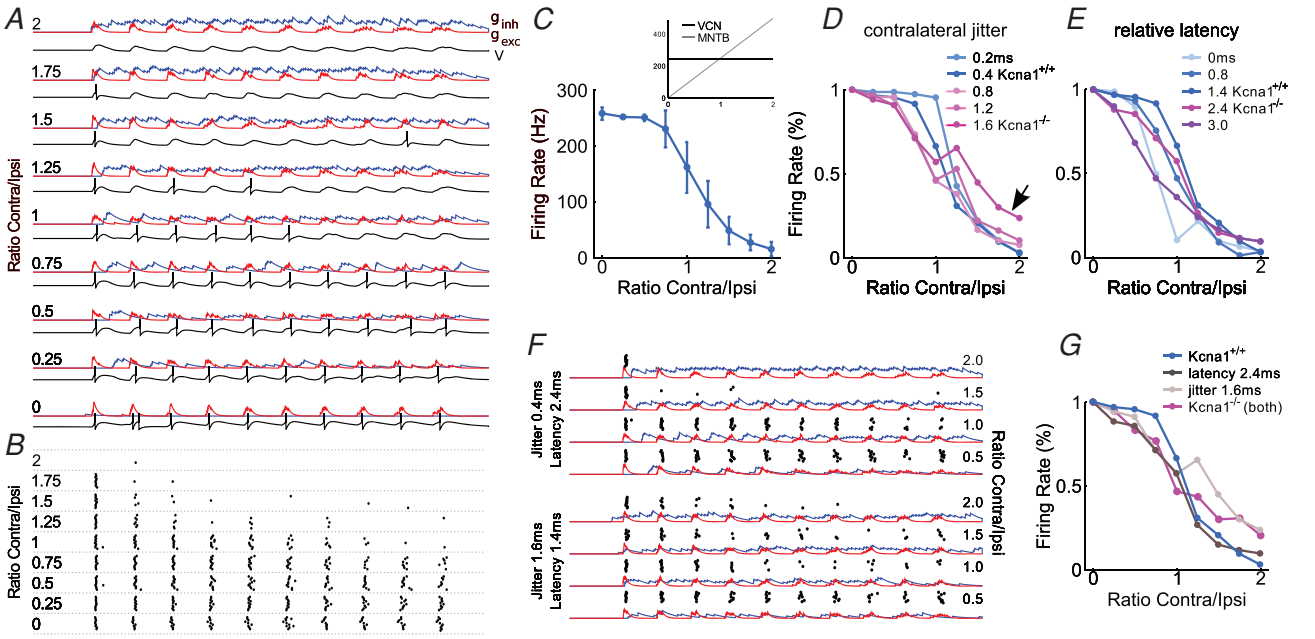


**Figure 4. Computational modelling of IID tuning in *Kcna1*$^{+/+}$ and *Kcna1*$^{-/-}$ LSO neurons**
*A*, excitatory (red, $g_{exc}$) and inhibitory (blue, $g_{inh}$) synaptic conductance and membrane potential (*V*, black trace below respective conductance traces) of an LSO neuron for different spike rates of the contralateral, inhibitory input (expressed as the ratio of contralateral and ipsilateral spike rates indicated on the left side). Parameters were: ipsilateral spike jitter S.D.0.15 ms, contralateral spike jitter S.D. 0.4 ms, relative mean latency 1.4 ms. *B*, APs (dots) of a simulated LSO neuron during 10 repetitions of a 40 ms stimulus under the conditions described in *A*. *C*, the resulting IID tuning curve of the simulated LSO neuron. The inset shows the firing rates of a prototypic VCN (black) and MNTB (grey) neuron for the respective input conditions. *D* and *E*, effects of changing the AP jitter (*D*) and first spike latency of spikes in the contralateral input (relative to the ipsilateral input) (*E*). All remaining parameters are the same as in *A*. Firing rate begins to decrease at lower contralateral rates in the presence of larger jitter and slopes of IID functions decrease. First-spike latency of contralateral spikes has a weaker influence on the response of the simulated LSO neuron. *F*, examples of simulated synaptic conductance and LSO spike trains (design same as in *A*) for an increased contralateral latency (top four traces) and jitter (bottom four traces). Dots indicate single APs. *G*, simulated IID tuning curves for the control case (as in *A*–*C*), for an increased contralateral jitter, for an increased latency, and for the combination of both. In all simulations, the ipsilateral input had a spike rate of 250 Hz, and the contralateral input was varied from 0 Hz (ratio = 0) to 500 Hz (ratio = 2).

LSO. This can be seen in the spike raster plots in Fig. 4*B*, illustrating that early spikes are not inhibited except for very high contralateral rates (i.e. short latency). Without a level-dependent latency decrease, these responses would not be inhibited at all (Park *et al.* 1997). Hence this model shows that both the ratio of contralateral and ipsilateral input strength and the timing of the APs in the respective input determine IID sensitivity.

These results suggest that a less effective inhibition due to lower maximum firing rates and longer latencies in the MNTB of *Kcna1*$^{-/-}$ mice could account for the observed insufficient inhibition in LSO neurons (Fig. 3*D*). Yet, it is still unclear why these LSO neurons typically favour positive IIDs (Fig. 3*E*), since a reduced inhibitory input from the MNTB would predict a shift towards more negative IIDs. Therefore, we investigated how increased AP jitter and latency in the contralateral inhibitory input could affect the IID-tuning properties of the simulated LSO neuron.

Simulations with different amounts of AP jitter in the contralateral input show that a modest jitter of 0.8 ms (i.e. wild-type) causes suppression of the LSO firing even at low contralateral spike rates (Fig. 4*D*). In the presence of stronger jitter (i.e. knockout) the IID functions begin to decrease at lower contralateral rates. As a consequence, the rate-dependent decrease of the IID function is shallower, and encoding of IIDs is less precise. This is caused by the increased temporal dispersion of inhibitory synaptic events, such that a temporally broadly distributed, but weak inhibition is present already at low contralateral firing rates (Fig. 4*F*, bottom). At the same time, increasing jitter also prevents full inhibition at high contralateral rates (Fig. 4*D*, arrow), because now inhibition no longer reliably coincides with excitatory events, especially for the early ipsilateral spikes (Fig. 4*F*, bottom). Overall, these effects are consistent with the tendency towards more positive IIDs, the loss of precise tuning and the lack of sufficient inhibition observed in *Kcna1*$^{-/-}$ mice (Fig. 3). It is also worth mentioning that averaging of IPSPs from multiple inhibitory inputs improves the tuning even in the presence of strong contralateral jitter. In the same simulations with just a single inhibitory input, IID tuning is almost completely abolished even at modest amounts of jitter (not illustrated).

Compared to the jitter, the first spike latency of contralateral spikes has a weaker influence on the response of the simulated LSO neuron, at least for modest changes (Fig. 4*E*). An increase in latency by up to a factor of two primarily prevents inhibition of early spikes, and hence prevents complete inhibition also during high contralateral rates. Only if the latency of one input is strongly increased or decreased, such that the excitatory and inhibitory synaptic inputs coincide again but at later cycles of the stimulus, do the IID functions become shallower and begin to drop already at low contralateral rates. In our simulations, such latency differences between the ipsi- and the contralateral input amount up to at least 3 ms, which is longer than the typical latency difference observed in *Kcna1*$^{-/-}$ mice. Therefore, it seems more likely that the genotype specific difference in the IID tuning is caused by an increase in the jitter of the contralateral inhibitory input rather than its latency. When both the contralateral jitter and latency are increased simultaneously, the effect is similar to that of an increase in jitter alone (Fig. 4*G*).

Finally, for strong jitter or small latencies, the IID curves show a second peak at a firing rate ratio of 1.25. This is caused by the de-synchronisation of the two spike trains due to the imposed rate difference, which is amplified in these cases because strong jitter renders inhibition less effective. It is unclear whether this effect is present in the data because the model actually predicts a weak effect (Fig. 4*G*), which would be difficult to separate from the overall variability of the experimentally measured tuning curves.

## Discussion

The importance of Kv1.1 containing channels for AP timing was used as a tool to study the contribution of precise onset firing to the encoding of sound source location based on the integration of interaural intensity differences (IIDs). We showed a lack of sensitivity to negative IIDs in mice lacking Kv1.1 containing channels, i.e. neurons in the knockout LSO preferably encode ipsilateral sound positions. Shallower slopes of individual IID functions in knockout LSO neurons resulted in more ambiguous and less precise IID encoding. The objective of our study was then to experimentally and computationally dissect whether temporal features or a change in the rate code along the excitatory and/or the inhibitory pathway caused the reduction in IID resolution. Our results suggest that Kv1.1 containing channels mediate a temporally precise onset inhibition which is required for correct encoding of sound source locations via IIDs in the mouse LSO.

### Possible contribution of axonal/dendritic Kv1.1 containing channels to IID tuning in *Kcna1*$^{-/-}$ mice

The contralateral inhibitory pathway significantly exceeds the ipsilateral excitatory one in axonal length. Extracellular recordings did not allow us to test how LSO neurons cope with the increased jitter of inhibitory responses directly. However, temporal accuracy in the LSO during ipsilateral excitatory stimulation was not significantly decreased suggesting that (a) the intrinsic properties of LSO neurons are only a little affected by the knockout and (b) that jitter arising along the axons can be compensated for by temporal summation of several inputs. In contrast,

the MNTB relies on one calyceal input and is therefore more susceptible to temporal ambiguity provided by the input. Indeed, effects on latency, jitter and firing rate were most pronounced for the inhibitory pathway and were already monitored at the level of the calyx of Held (Kopp-Scheinpflug *et al.* 2003). These effects are likely to originate from the lack of Kv1.1-containing channels in the juxtaparanodal regions of the nodes of Ranvier along the axons (Wang *et al.* 1993; Rasband & Trimmer, 2001).

Regenerative axonal APs are characterized by a prominent depolarizing after-potential thought to result from the partial discharge of the internodal membrane caused by nodal currents during an AP (for review see: Baker, 2000). In *Kcna1*$^{-/-}$ mice, Kv1 channels in the juxtaparanodal regions, which usually provide sufficient outward currents, might fail to limit nodal depolarization. Thus, as suggested by Gittelman & Tempel (2006), during ongoing AP firing in *Kcna1*$^{-/-}$ axons the resting membrane potential would depolarize slightly and inactivate sodium channels at the nodes of Ranvier (Leao & Von Gersdorff, 2002), thereby reducing the number of APs. A slight imperfection in the use of knockout mice is the possibility of compensation, in this case by other Kv1 channel subunits, i.e. Kv1.2 or Kv1.6. Voltage-clamp experiments in brain slices of *Kcna1*$^{-/-}$ mice showed dendrotoxin-sensitive potassium currents to be reduced compared to wild-type currents (Brew *et al.* 2003), suggesting possible compensation to be incomplete. Another approach to studying Kv1.1 function uses a point mutation in the *Kcna1* gene which results in a more severe phenotype most likely because wild-type Kv1.2 or Kv1.6 subunits become non-functional due to their heteromultimerization with mutant Kv1.1 subunits (Herson *et al.* 2003). In this case, however, the phenotype is so strong that the homozygote mutants die embryonically and only heterozygotes can be studied. It would therefore be interesting to elucidate the contribution of Kv1.1 containing channels to axonal conduction in future work.

Jitter in the inhibitory input causes lack of IID sensitivity corresponding to contralateral sound positions.

We were unable to entirely clarify why *Kcna1*$^{-/-}$ units appear to exclusively encode positive IIDs. The presence of IID functions in both genotypes shows that the general anatomical circuit has not failed to develop in the absence of the *Kcna1* gene; excitation is conveyed by ipsilateral stimulation and inhibition by contralateral stimulation. However, the limitation of IID sensitivity to positive IIDs, where lower inhibitory stimulus intensity is necessary to suppress the ipsilaterally evoked firing, seemed unexpected. The severely affected signal processing in the MNTB intuitively supported the hypothesis of a shift of IID functions towards negative IIDs requiring more intense inhibitory stimuli to compensate for the delay and the lower firing rate (Kopp-Scheinpflug *et al.* 2003). As reported by Park *et al.* (1996), there are two possibilities for LSO cells to encode negative IIDs: in neurons with matched latencies for excitatory and inhibitory inputs of equal strength, threshold of the inhibitory input ought to be higher, while in neurons with a temporal mismatch of the excitatory and inhibitory inputs, longer latencies of the inhibitory input would cause sensitivity to negative IIDs. In both cases, a more intense inhibitory stimulus would be necessary to reduce firing rate to trade time for intensity (Pollak, 1988; Grothe & Park, 1995). We conclude that *Kcna1*$^{-/-}$ neurons that are configured to matched latencies would not receive a proper input because of the increased latency and jitter of the inhibitory input and thus fail to encode negative IIDs. In neurons with mismatched latencies, again the additional delay of the MNTB responses might prevent the inhibition from being effective.

Both of the above scenarios lead to the inability to suppress 50% or more of ipsilaterally evoked firing rate in the range of negative IIDs. Neurons that showed inhibition weaker than 50% were not included in the comparison of $IID_{50}$ values. Increased thresholds in the *Kcna1*$^{-/-}$ mice and the limitation of the loudspeaker output to 90 dB SPL did not allow a further increase in intensity to compensate (trade) for the delayed latencies without encountering a ceiling effect. An alternative strategy to test the hypothesis of the delayed inhibitory input was to allow the inhibitory stimulus to start early compared to the excitation. Following the paradigm of time–intensity trading (Pollak, 1988), the presentation of the contralateral stimulus in advance to compensate for the delayed inhibitory input caused those *Kcna1*$^{-/-}$ neurons to regain sensitivity to negative IIDs (Supplemental Material). This demonstrates that in *Kcna1*$^{-/-}$ neurons delayed inhibition could cause the lack of negative IIDs.

## Insights from the computational model

Our computational model could reliably reproduce the shallower slopes along with significantly broader dynamic ranges of IID functions, the reduction of firing rates already at lower contralateral stimulus intensities and the less effective inhibition for high contralateral stimulus intensities in *Kcna1*$^{-/-}$ units. These effects could all be attributed to the substantial AP jitter in the contralateral input. The analysis of the model further showed that differences in IID tuning are most likely to be due to different matched combinations of the intensity–response relationships for the two inputs. A more negative IID, for instance, would require a weaker increase of the intensity–response curve for the contralateral input. This finding is consistent with earlier proposals by Reed & Blum (1990) and Park *et al.* (1996).

Specifically, the model shows that precisely timed inhibition is required for effective IID tuning. While this is the case in wild-type mice, where the inhibitory

PSPs from the MNTB show little temporal jitter, IPSPs in *Kcna1*$^{-/-}$ units are substantially spread out in time, thereby reducing the effectiveness of inhibition. At the same time, this increases the probability of inhibition even for low contralateral rates, which would normally have no effect because then ipsilateral EPSCs and contralateral IPSCs do not coincide. As a result, IID tuning curves begin to drop at lower contralateral firing rates in simulated *Kcna1*$^{-/-}$ units, and complete inhibition cannot be achieved. A comparison also showed that differences in absolute latency are less important for these effects; they rely primarily on the increased spike jitter. This finding might explain why this impairment cannot be compensated for, since in this case information about the true IID is irreversibly lost along the pathway from the contralateral ear and cannot be restored at a later stage. For instance, compensation through LSO-intrinsic changes of excitability involving Kv channels in the knockout is very unlikely to recover the original IID tuning. Therefore, we did not further explore potential effects of the different intrinsic properties in the knockouts that might change synaptic integration in LSO neurons themselves.

### Behavioural relevance of precise onset timing in IID processing

The significance of submillisecond timing for IID encoding is not well understood. Precisely timed inhibitory inputs have been shown not to be required for IID encoding in the sustained response of LSO neurons. However, timing has been implied to be important for generating IID sensitivity at the stimulus onset as well as in LSO neurons tuned to low-frequency sounds (Park *et al.* 1996, Irvine *et al.* 2001). Studies using correlated *vs.* uncorrelated noise to evaluate the contribution of temporal acuity to IID sensitivity show subtle differences between the two conditions that could be explained by differences in temporal information available for IID processing (e.g. Fig. 8 in Tollin & Yin, 2002). When studying the onset rather than the ongoing IID sensitivity, temporally precise inhibition will cause a sudden reduction of the ipsilateral rates resulting in a small dynamic range of the IID functions and unambiguous IID coding. Less efficient inhibition will need longer (or be stronger activated) to reduce the ipsilateral rates. This results in larger dynamic ranges of the IID functions and more ambiguous IID coding. The combination of reduced maximum firing rates and increased jitter of the inhibitory input into the LSO diminishes the extent of IPSP summation resulting in less effective inhibition and a limitation if IID sensitivity corresponding to only one hemifield. From the perspective of the inferior colliculus (IC), which integrates the information from both LSOs, each LSO provides the encoding of only one hemisphere in *Kcna1*$^{-/-}$ mice. Integration of the two datasets in the IC might reflect the complete azimuth, but with only half the resolution. This then results in severely limited behavioural performance of sound source discrimination tasks in mice lacking the *Kcna1* gene (Allen *et al.* 2003) although more general auditory tasks were performed without obvious restrictions (Allen *et al.* 2008).

## References


Adams JC (1981). Heavy metal intensification of DAB-based HRP reaction product [letter]. *J Histochem Cytochem* **29**, 775.

Allen PD, Bell J, Dargani N, Moore CA, Tyler CM & Ison JR (2003). Kcna1 knockout mice have a profound deficit in discriminating sound source location. Society for Neuroscience, Washington, DC, Abstract 29:183.

Allen PD, Schmuck N, Ison JR & Walton JP (2008). Kv1.1 channel subunits are not necessary for high temporal acuity in behavioral and electrophysiological gap detection. *Hear Res* **246**, 52–58.

Baker MD ( 2000). Axonal flip-flops and oscillators. *Trends Neurosci* **23**, 514–519.

Bal R & Oertel D (2001). Potassium currents in octopus cells of the mammalian cochlear nucleus. *J Neurophysiol* **86**, 2299–2311.

Barnes-Davies M, Barker MC, Osmani F & Forsythe ID (2004). Kv1 currents mediate a gradient of principal neuron excitability across the tonotopic axis in the rat lateral superior olive. *Eur J Neurosci* **19**, 325–333.

Boudreau JC & Tsuchitani C (1970). Cat superior olive S-segment cell discharge to tonal stimulation. *Contrib Sens Physiol* **4**, 143–213.

Brew HM & Forsythe ID (1995). Two voltage-dependent $K^+$ conductances with complementary functions in postsynaptic integration at a central auditory synapse. *J Neurosci* **15**, 8011–8022.

Brew HM, Hallows JL & Tempel BL (2003). Hyperexcitability and reduced low threshold potassium currents in auditory neurons of mice lacking the channel subunit Kv1.1. *J Physiol* **548**, 1–20.

Cao XJ, Shatadal S & Oertel D (2007). Voltage-sensitive conductances of bushy cells of the Mammalian ventral cochlear nucleus. *J Neurophysiol* **97**, 3961–3975.

Chen QC, Cain D & Jen PH (1995). Sound pressure transformation at the pinna of *Mus domesticus*. *J Exp Biol* **198**, 2007–2023.

Dorrscheidt GH (1981). The statistical significance of the peristimulus time histogram (PSTH). *Brain Res* **220**, 397–401.

Finlayson PG & Caspary DM (1991). Low-frequency neurons in the lateral superior olive exhibit phase-sensitive binaural inhibition. *J Neurophysiol* **65**, 598–605.

FitzGerald JV, Burkitt AN, Clark GM & Paolini AG (2001). Delay analysis in the auditory brainstem of the rat: comparison with click latency. *Hear Res* **159**, 85–100.

Gittelman JX & Tempel BL (2006). Kv1.1-containing channels are critical for temporal precision during spike initiation. *J Neurophysiol* **96**, 1203–1214.

Glendenning KK, Hutson KA, Nudo RJ & Masterton RB (1985). Acoustic chiasm II: Anatomical basis of binaurality in lateral superior olive of cat. *J Comp Neurol* **232**, 261–285.

Grigg JJ, Brew HM & Tempel BL (2000). Differential expression of voltage-gated potassium channel genes in auditory nuclei of the mouse brainstem. *Hear Res* **140**, 77–90.

Grothe B & Park TJ (1995). Time can be traded for intensity in the lower auditory system. *Naturwissenschaften* **82**, 521–523.

Herson PS, Virk M, Rustay NR, Bond CT, Crabbe JC, Adelman JP & Maylie J (2003). A mouse model of episodic ataxia type-1. *Nat Neurosci* **6**, 378–383.

Irvine DR, Park VN & McCormick L (2001). Mechanisms underlying the sensitivity of neurons in the lateral superior olive to interaural intensity differences. *J Neurophysiol* **86**, 2647–2666.

Irvine DRF ( 1992). Physiology of the auditory brainstem. In *The Mammalian Auditory Pathway: Neurophysiology*, ed. Popper AN & Fay RR, pp. 153–231. Springer Verlag, Berlin, Heidelberg, New York.

Joris PX & Yin TC (1995). Envelope coding in the lateral superior olive. I. Sensitivity to interaural time differences. *J Neurophysiol* **73**, 1043–1062.

Kandler K, Clause A & Noh J (2009). Tonotopic reorganization of developing auditory brainstem circuits. *Nat Neurosci* **12**, 711–717.

Klug A & Trussell LO (2006). Activation and deactivation of voltage-dependent $K^+$ channels during synaptically driven action potentials in the MNTB. *J Neurophysiol* **96**, 1547–1555.

Kopp-Scheinpflug C, Fuchs K, Lippe WR, Tempel BL & Rubsamen R (2003). Decreased temporal precision of auditory signaling in Kcna1-null mice: an electrophysiological study in vivo. *J Neurosci* **23**, 9199–9207.

Kuwabara N & Zook JM (1992). Projections to the medial superior olive from the medial and lateral nuclei of the trapezoid body in rodents and bats. *J Comp Neurol* **324**, 522–538.

Leao RM & Von Gersdorff H (2002). Noradrenaline increases high-frequency firing at the calyx of held synapse during development by inhibiting glutamate release. *J Neurophysiol* **87**, 2297–2306.

Lorincz A & Nusser Z (2008). Cell-type-dependent molecular composition of the axon initial segment. *J Neurosci* **28**, 14329–14340.

Manis PB & Marx SO (1991). Outward currents in isolated ventral cochlear nucleus neurons. *J Neurosci* **11**, 2865–2880.

Oertel D, Shatadal S & Cao XJ (2008). In the ventral cochlear nucleus Kv1.1 and subunits of HCN1 are colocalized at surfaces of neurons that have low-voltage-activated and hyperpolarization-activated conductances. *Neuroscience* **154**, 77–86.

Ollo C & Schwartz IR (1979). The superior olivary complex in C57BL/6 mice. *Am J Anat* **155**, 349–373.

Osen KK (1969). Cytoarchitecture of the cochlear nuclei in the cat. *J Comp Neurol* **136**, 453–484.

Park TJ, Grothe B, Pollak GD, Schuller G & Koch U (1996). Neural delays shape selectivity to interaural intensity differences in the lateral superior olive. *J Neurosci* **16**, 6554–6566.

Park TJ, Monsivais P & Pollak GD (1997). Processing of interaural intensity differences in the LSO: role of interaural threshold differences. *J Neurophysiol* **77**, 2863–2878.

Pollak GD (1988). Time is traded for intensity in the bat's auditory system. *Hear Res* **36**, 107–124.

Rasband MN & Trimmer JS (2001). Developmental clustering of ion channels at and near the node of Ranvier. *Dev Biol* **236**, 5–16.

Reed MC & Blum JJ (1990). A model for the computation and encoding of azimuthal information by the lateral superior olive. *J Acoust Soc Am* **88**, 1442–1453.

Sanes DH (1990). An in vitro analysis of sound localization mechanisms in the gerbil lateral superior olive. *J Neurosci* **10**, 3494–3506.

Sanes DH & Takacs C (1993). Activity-dependent refinement of inhibitory connections. *Eur J Neurosci* **5**, 570–574.

Smart SL, Lopantsev V, Zhang CL, Robbins CA, Wang H, Chiu SY, Schwartzkroin PA, Messing A & Tempel BL (1998). Deletion of the K(V)1.1 potassium channel causes epilepsy in mice. *Neuron* **20**, 809–819.

Smith PH, Joris PX, Carney LH & Yin TC (1991). Projections of physiologically characterized globular bushy cell axons from the cochlear nucleus of the cat. *J Comp Neurol* **304**, 387–407.

Smith PH, Joris PX & Yin TC (1998). Anatomy and physiology of principal cells of the medial nucleus of the trapezoid body (MNTB) of the cat. *J Neurophysiol* **79**, 3127–3142.

Spangler KM, Warr WB & Henkel CK (1985). The projections of principal cells of the medial nucleus of the trapezoid body in the cat. *J Comp Neurol* **238**, 249–262.

Tollin DJ (2003). The lateral superior olive: a functional role in sound source localization. *Neuroscientist* **9**, 127–143.

Tollin DJ, Koka K & Tsai JJ (2008). Interaural level difference discrimination thresholds for single neurons in the lateral superior olive. *J Neurosci* **28**, 4848–4860.

Tollin DJ & Yin TC (2002). The coding of spatial location by single units in the lateral superior olive of the cat. I. Spatial receptive fields in azimuth. *J Neurosci* **22**, 1454–1467.

Trussell LO (1999). Synaptic mechanisms for coding timing in auditory neurons. *Annu Rev Physiol* **61**, 477–496.

Tsai JJ, Koka K & Tollin DJ (2010). Varying overall sound intensity to the two ears impacts interaural level difference discrimination thresholds by single neurons in the lateral superior olive. *J Neurophysiol* **103**, 875–886.

Wang H, Kunkel DD, Martin TM, Schwartzkroin PA & Tempel BL (1993). Heteromultimeric $K^+$ channels in terminal and juxtaparanodal regions of neurons. *Nature* **365**, 75–79.

Wang H, Kunkel DD, Schwartzkroin PA & Tempel BL (1994). Localization of Kv1.1 and Kv1.2, two K channel proteins, to synaptic terminals, somata, and dendrites in the mouse brain. *J Neurosci* **14**, 4588–4599.

Wu SH & Kelly JB (1991). Physiological properties of neurons in the mouse superior olive: membrane characteristics and postsynaptic responses studied in vitro. *J Neurophysiol* **65**, 230–246.

Yin TC (2002). Neural mechanisms of encoding binaural localization cues in the auditory brainstem. In *Integrative Functions in the Mammalian Auditory Pathway*, ed. Oertel D, Popper AN & Fay RR, pp. 99–159. Springer-Verlag, New York.

## Author contributions

A.K. conducted most experiments, analysed all the data and wrote the first draft of the article. M.H.H. developed the computational model and wrote parts of the article. C.A.R. conducted immunocytochemistry for Kv1.1, Kv1.2 and the $Na_V$ in the LSO. B.L.T. generated and provided *Kcna1*$^{-/-}$ mice, advised on the design of immunocytochemical experiments and revised article. R.R. advised on experimental design of electrophysiological experiments and revised the article. C.K.S. conceived project, designed and conducted experiments, and wrote the article. All authors approved the final version of the manuscript for publication.

## Author's present address

C. Kopp-Scheinpflug: MRC Toxicology Unit, University of Leicester, Leicester, UK.

## Acknowledgements

We are very grateful to I. D. Forsythe, J. Ison and C. O'Donnell for helpful comments on an earlier version of this manuscript. We also like to thank N. Froehlich and D. Freyberg for helping with mouse handling and genotyping. This work was supported by the German Academic Exchange Service DAAD-D/07/40536 (A.K.) and Graduate School 1097 funded by the German Research Council (DFG) (A.K.), a UK Medical Research Council fellowship (G0501327, M.H.H.), the NIH (DC002739, B.L.T., C.A.R.), the DFG (390/18-2 and 390/19-1, R.R.) and by a HSP3-Habilitation-Fellowship of the Saxonian Government and the Schmitt Program on Integrative Brain Research (C.K.S.).